Supporting Information

Pd-catalyzed Instant Hydrogenation of TiO_2 with Enhanced Photocatalytic Performances

Yingfeng Xu, Chen Zhang, Lingxia Zhang, Xiaohua Zhang, Heliang Yao and Jianlin Shi*

State Key Laboratory of High Performance Ceramics and Superfine Microstructure, Shanghai Institute of Ceramics, Chinese Academy of Sciences, Shanghai, 200050, P. R. China.

E-mail: jlshi@mail.sic.ac.cn

1. Supplementary Methods

Materials

Tetrabutyltitanate (TBOT, 97%), sodium tetrachloropalladate (II) (Na_2PdCl_4, 99%), Palladium(II) acetylacetonate ($Pd(AcAc)_2$), polyvinylpyrrolidone (Average MW 40000, PVP) were purchased from Sigma-Aldrich. Hydrofluoric acid (HF, 47%), hydrochloric acid (HCl, 37%), ethylene glycol (EG, 99%), methanol (99%), acetone (95%), ethanol (95%) and methylene blue trihydrate (MB) were obtained from Sinopharm Chemical Reagent Co., Ltd, China. α-Al_2O_3 powders were purchased from Alfa Aesar. All the chemicals were used as received without further purification. Deionized water used throughout the experiments was prepared using ELGA water purification system (PURELAB Classic).

Pd-catalyzed hydorgenation of the series TiO_2 samples

(1) Preparation of pristine TiO_2 samples

Pure rutile TiO_2 nanoparticles, labeled as R, pure anatase TiO_2 nanoparticles, labeled as A, and TiO_2 films, labeled as TiO_2-F were synthesized by the sol-hydrothermal method according to the previous literatures respectively.[1-3] In brief, rutile TiO_2 samples were synthesized by adding 5 ml TBOT into 100 ml of 1.5 M HCl aqueous solution in a 120 ml Teflon-lined stainless-steel autoclave, which was kept at 200 °C for 48 h. Anatase TiO_2 samples were synthesized by mixing 10 ml of TBOT and 1.2 ml of HF into a 40 ml Teflon-lined stainless-steel autoclave, which was kept at 180 °C for 24 h. TiO_2 films grown on FTO glass substrates was prepared by adding four clean FTO glass substrate into 30 ml of 6 M HCl aqueous solution containing 0.6 ml of TBOT in a 80 ml Teflon-lined stainless-steel autoclave, which was kept at 150 °C for 6 h.

(2) Preparation of Pd-loaded TiO_2 samples

All of the chemical reagents of analytical grade were purchased from Sigma-Aldrich and used as received without further purification. Pd-loaded rutile/anatase TiO_2 nanoparticles, labeled as R/Pd or A/Pd, respectively, was prepared by a solvothermal method. Typically, 500 mg of the as-synthesized R/A powder was dispersed into 100 ml of ethylene glycol under ultrasonication. Then, 5 ml of 10 mM Na_2PdCl_4 aqueous solution was added in the solution and stirred at room temperature for 6 h under dark condition. After addition of 1 g PVP, the mixture was stirred for another 1 h, and transferred to a 250 ml flask, heated to 150 °C under vigorous stirring. Afterward,

the solution was cooled to room temperature naturally, the product was collected by centrifuged, washed with water and ethanol for several times, vacuum-dried and calcined at 500 °C for 2 h to completely remove the residual organics. Additionally, Ag, Pt, Au-loaded rutile TiO_2 were also prepared with the same process by adding $AgNO_3$, H_2PtCl_6, $HAuCl_4$ respectively (labeled as TiO_2/Ag, TiO_2/Pt and TiO_2/Au). As controls, the as-synthesized rutile and anatase TiO_2 nanoparticles were treated with the same process without the addition of Na_2PdCl_4 aqueous solution. Decoration of Pd nanoparticles on TiO_2 nanowires film, labeled as TiO_2-F/Pd, was performed by a photocatalytic reduction method. Typically, the prepared TiO_2-F samples were soaked into 10 ml of 1mM $Pd(AcAc)_2$ aqueous solution in a quartz vessel. After being bubbled with N_2 to remove air completely, the vessel was irradiated by a 300 W Xe lamp for 30 min. Then the obtained TiO_2-F/Pd samples were thoroughly rinsed with deionized water and annealed in air at 400 °C for 1 h. As control, TiO_2-F samples were treated under the same condition with pure water instead of $Pd(AcAc)_2$ solution.

(3) Pressureless hydrogen treatment of different TiO_2 samples at room temperature

Ambient H_2/Ar gas flow treated R/Pd (A/Pd, TiO_2-F/Pd) with or without oxygen is labeled as O&H-R/Pd (O&H-A/Pd, O&H-TiO_2-F/Pd) and H-R/Pd (H-A/Pd, H-TiO_2-F/Pd), respectively. Typically, H-R/Pd (H-A/Pd) or H-TiO_2-F/Pd was prepared through treating 200 mg R/Pd (A/Pd) or TiO_2-F/Pd samples in 200 sccm H_2/Ar (10 vol% H_2) gas flow at room temperature for 10 min, which was performed in an alumina crucible located at the center of a glass tube. As to the oxygen-assisted Pd-catalyzed hydrogenation process, 2 vol% O_2 was added into the H_2/Ar gas flow under the same condition, O&H-R/Pd (O&H-A/Pd, O&H-TiO_2-F/Pd) samples were obtained. As controls, pure rutile and anatase TiO_2 samples were treated under the same conditions and labeled as H-R, O&H-R, H-A and O&H-A, respectively. Additionally, 200 mg of the TiO_2/Ag, TiO_2/Pt and TiO_2/Au samples were also treated with 200 sccm H_2/Ar (10 vol% H_2) gas flow for 30 min at room temperature.

Hydrogen treatment on Pd-loaded α-Al_2O_3

Since α-Al_2O_3 is of high stability and cannot be reduced, the same hydrogen treatment as abovementioned on TiO_2 species was performed on α-Al_2O_3 in the presence of Pd, as negative control to investigate the potential effects of Pd nannoparticles on the EPR results and the photocatalytic hydrogen evolution after the hydrogen treatment. Therefore, the similar

solvothermal reduction approach that used for synthesizing R-TiO_2/Pd sample described above was conducted to obtain Pd loaded α-Al_2O_3 (Al_2O_3/Pd) sample. Then, the hydrogen treatment of 200 mg Al_2O_3/Pd was performed under a 200 sccm H_2/Ar (10 vol% H_2) with or without 2 vol% O_2 gas flow at room temperature for 30 min, labeled as O&H-Al_2O_3/Pd and H-Al_2O_3/Pd, respectively.

Generalization of the Pd-catalyzed hydorgenation strategy to other transition metal oxides

(1) CeO_2 nanowires synthesis and corresponding Pd-catalyzed hydrogenation treatments

The CeO_2 nanowires were synthesized according to the previously reported procedure with a little improvement.[4] Firstly, 1 ml of 2 mM $Ce(NO_3)_3 \cdot 6H_2O$ was dropwise added into 40 ml of 10 M NaOH aqueous solutions under continuous stirring. After a vigorous stirring for 1 h at room temperature, the solution was transferred into the Teflon-lined autoclaves (80 ml) for 20 h at 120 °C. After naturally cooling to room temperature, the precipitates were collected by centrifuge, washed with deionized water for three times and freeze-dried under vacuum. Then, the similar solvothermal reduction approach that used for synthesizing R-TiO_2/Pd sample described above was conducted to obtain Pd loaded CeO_2 (CeO_2/Pd) sample. And 200 mg of the prepared CeO_2/Pd and CeO_2 powder was treated under 200 sccm H_2/Ar (10 vol%) gas flow at room temperature for 30 min, labeled as H-CeO_2/Pd and H-CeO_2 respectively.

(2) WO_3 microrods synthesis and corresponding Pd-catalyzed hydrogenation treatments

The WO_3 microrods were synthesized according to the previously reported procedure with a little improvement.[5] 3 mmol WCl_6 was firstly dissolved in 50 ml of acetic acid, afterwards 1 ml deionized water was added and stirred for 30 min at room temperature. The solution was transferred to a Teflon-lined stainless steel autoclave (80 ml) and heated at 180 °C for 12 h. After naturally cooling to room temperature, the resultant powders were separated via centrifugation, washed with deionized water for three times, and finally freeze-dried under vacuum. Then, the similar solvothermal reduction approach that used for synthesizing R-TiO_2/Pd sample described above was conducted to obtain Pd loaded WO_3 (WO_3/Pd) sample. And 200 mg of the prepared WO_3/Pd and WO_3 powder was treated under 200 sccm H_2/Ar (10 vol%) gas flow at room temperature for 30 min, labeled as H-WO_3/Pd and H-WO_3 respectively.

Material characterizations

X-ray diffraction (XRD) measurement was carried out on a Bruker D8 ADVANCE powder diffractometer at Cu Kα (λ = 0.154056 nm) with a scanning rate of 4°/min in the 2θ range of 10-

80°. Raman scattering was measured by a LABRAM-HR micro-Raman spectrometer with laser excitation energy of 514 nm, and the laser beam was focused with a 50 × objective lens to a ca.1 μm spot on the surface of the sample. Transmission electron microscope (TEM) images coupled to electron energy loss spectroscopy (EELS) were acquired on a JEM-2100F equipped with a Gatan GIF 963 operated at 200 kV, and the lattice structural analysis was done using the Digital Micrograph software. Scanning electron microscopy (SEM) images and energy-dispersive X-ray analysis (EDS) were performed on FEI Magellen 400. The quantitative analysis of element contents in nanoparticles are performed with Agilent 700 Series inductively coupled plasma optical emission spectrometry (ICP-OES). The diffuse reflectance spectra of the samples were recorded on a Hitachi U4100 spectrophotometer. X-ray photoelectron spectroscopy (XPS) experiments were carried out on a Thermo Scientific ESCALAB 250 spectrometer with a monochromated Al Kα source (hν= 1486.6ν eV). Accurate binding energies (± 0.1 eV) were determined with respect to the position of the adventitious C 1 s peak at 284.8 eV. The deconvolution of the Ti and O peaks was performed through a software XPSPEAK version 4.1, and the energy scales of valance band XPS (VBXPS) are aligned by using the Fermi level of the XPS instrument. The electron paramagnetic resonance (EPR) spectra were recorded on a continuous wave X-band JES-FA200 EPR spectrometer with a microwave power of 1 mW. Mn-Marker was used as an internal standard for the measurement of the magnetic field. The microwave frequency was 9.066 GHz and every spectrum was integrated over three sweeps of the applied field from 0 to 800 mT. In each measurement, 50 mg of the sample was placed in a quartz EPR tube and measured at 100K.

Photocatalytic activity measurements

(1) Photocatalytic decomposition of methylene blue (MB)

In a typical experiment, 50 mg of catalyst was dispersed in 100 ml of MB (10 mg l^{-1}) in a quartz cell reactor, which was then sonicated for 5 min and stirred in dark for 4 h to establish adsorption-desorption equilibrium before irradiation. Next, the solutions were irradiated with a 300 W Xe light source through an Air Mass 1.5 G filter (ca. 100 mW cm^{-2}) at room temperature and bubbled with O_2 at a fixed flow rate along with magnetic stirring. Then at different time points, 2 ml of aliquot was collected and centrifuged to obtain a transparent solution, and the residual MB concentration was measured by a Hitachi UV-3100 UV-Vis-NIR spectrophotometer through

monitoring the optical absorption at ~660nm.

(2) Photocatalytic hydrogen evolution from water reduction

Photocatalytic water reduction with methanol as the sacrificial reagent were conducted in a top-irradiation-type quartz reaction vessel under the irradiation of a 300 W Xe lamp with an Air Mass 1.5 G filter (AM 1.5 G, ca. 100 mw cm^{-2}) or an optical UV cut-off filter (λ>400 nm, ca. 85 mw cm^{-2}). 50 mg of catalyst was suspended in 100 ml 20 vol% methanol aqueous solution, which was then sonicated for 10 min. After being bubbled with N_2 to remove air completely, the reactant solution was irradiated by the Xe lamp at a constant temperature of 10 °C under stirring. The evolved gas was withdrawn every 1 h by a syringe and analyzed by a gas chromatography (GC7900, Tianmei, Shanghai, TCD, nitrogen as a carrier gas and 5 Å molecular sieve column). To minimize the experimental errors and ensure the credibility of the results, every cycling of the photocatalytic hydrogen evolution experiment was repeated for three times. And for H-R/Pd (H-A/Pd) and O&H-R/Pd (O&H-A/Pd), it started from the hydrogen treatment of R/Pd (A/Pd) samples. The experimental error in every photocatalytic H_2 evolution test was within 15 %. H-Al_2O_3/Pd and O&H-Al_2O_3/Pd samples were also measured under the same conditions and no H_2 gas can be detected, excluding the possible reason of Pd and H complex for the observed performance improvements. The cycling tests of H-R/Pd (H-A/Pd) and O&H-R/Pd (O&H-A/Pd) in hydrogen evolution experiments were conducted for 10 consecutive days; the sample was irradiated for 5 hours each day and then stored in darkness overnight before testing the next day.

Photoelectrochemical measurements

The series of TiO_2-F samples (TiO_2-F, TiO_2-F/Pd, H-TiO_2-F/Pd, O&H-TiO_2-F/Pd) were fabricated into photoanodes by soldering a copper wire onto a bare part of the FTO substrate and sealing the substrate edges and the metal contact regions with insulating epoxy resin. The working electrode areas of the photoanodes are 0.25 cm^2. Photoelectrochemical (PEC) performances of the prepared photoanodes were evaluated in a typical undivided three-electrode configuration (an Ag/AgCl electrode reference electrode and a Pt foil counter electrode) using a Solartron 1287 electrochemical interface analysis instrument operated by the CorrWare program. 1 M NaOH (pH = 13.6) purged with N_2 was used as the electrolyte. The measured potentials vs. Ag/AgCl were converted to reversible hydrogen electrode (RHE) scale via the Nernst equation $E_{RHE} = E_{Ag/AgCl} + 0.197 + 0.059pH$. A 300 W Xe arc lamp coupled with an AM 1.5G filter (100 mW cm^{-2}) was

applied as the simulated sunlight source. Typically, *J-V* curves were measured at a scan rate of 5 mV s^{-1} and the chopped illumination was used to examine transient photocurrents. Transient photocurrent measurements at a constant bias (0.5 V vs. RHE) with chopped illumination were also conducted to examine the steady-state photocurrent densities of the photoanodes. Electrochemical impedance spectra (EIS) were carried out in the frequency range of 10 to 10^6 Hz with an AC voltage amplitude of 5 mV at a DC bias voltage of 0.25 V vs. RHE under illumination. Mott-Schottky plots were measured at a frequency of 5 kHz under dark condition.

The incident photon-to-current efficiency (IPCE) was measured at 1.0 V vs. RHE using a specially designed IPCE system for solar cell with three-electrode configuration. A solar simulator (Newport 69907, 150 W Xenon lamp) coupled with an aligned monochrometor (Oriel Cornerstone 130 1/8 m) was used to generate a monochromatic beam. The incident light intensity was calibrated by a standard silicon photodiode detector. IPCE under each wavelength is determined by the equation:

$$\mathrm{IPCE}(\lambda) = \frac{1240I}{\lambda J_{light}}$$

where λ is the wavelength of incident beam, I is the photocurrent density at each specific wavelength and J_{light} is the irradiance at each specific wavelength.

2. Supplementary Tables and Figures

Table S1. ICP-AES results of noble metal doping amount (mol% to the corresponding metal element) in all the samples involved.

Sample	TiO_2/Pd	TiO_2/Ag	TiO_2/Pt	TiO_2/Au	R/Pd	A/Pd	TiO_2-F/Pd	CeO_2/Pd	WO_3/Pd	Al_2O_3/Pd
noble metal mol%	1.324	1.894	1.761	1.705	0.431	0.482	1.357	0.736	0.577	1.535

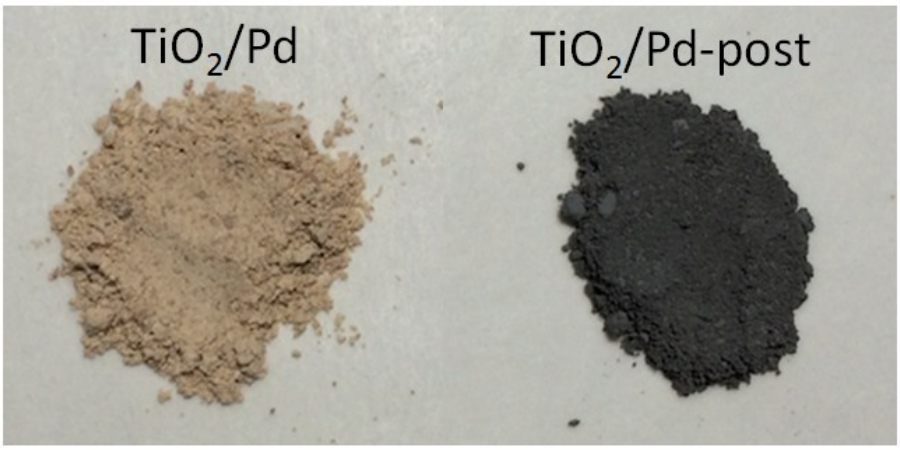

Figure S1. Photographs of TiO_2/Pd powders before and after (TiO_2/Pd-post) the photocatalytic hydrogen evolution experiment. The colour of TiO_2/Pd sample changed immediately from yellow to black during the hydrogen evolution experiment, and the black colour remained stable even stored in air or aqueous solution for weeks.

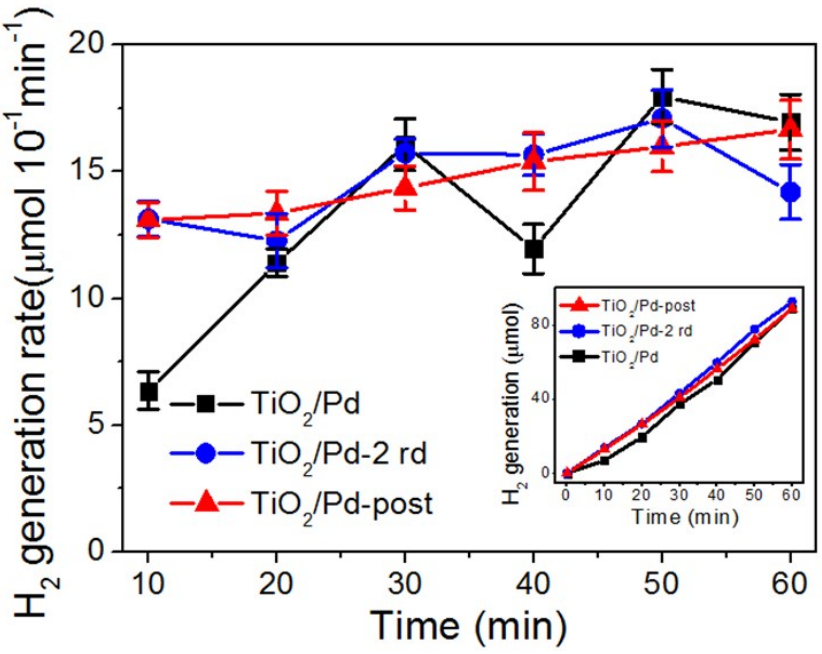

Figure S2. Amount of photocatalytic hydrogen production in every 10 min of TiO_2/Pd during and after the self-reduction, the insert is the time-course record of hydrogen generation. The hydrogen generation rate of TiO_2/Pd enhanced about two-fold after the first 10 min illumination, which was maintained in the successive second round test (TiO_2/Pd-2rd) or in a new round test by recycling the colour-changed TiO_2/Pd powders (TiO_2/Pd-post), indicating that the potential changed chemical properties of TiO_2 during the hydrogen evolution experiment could enhance its photocatalytic performance.

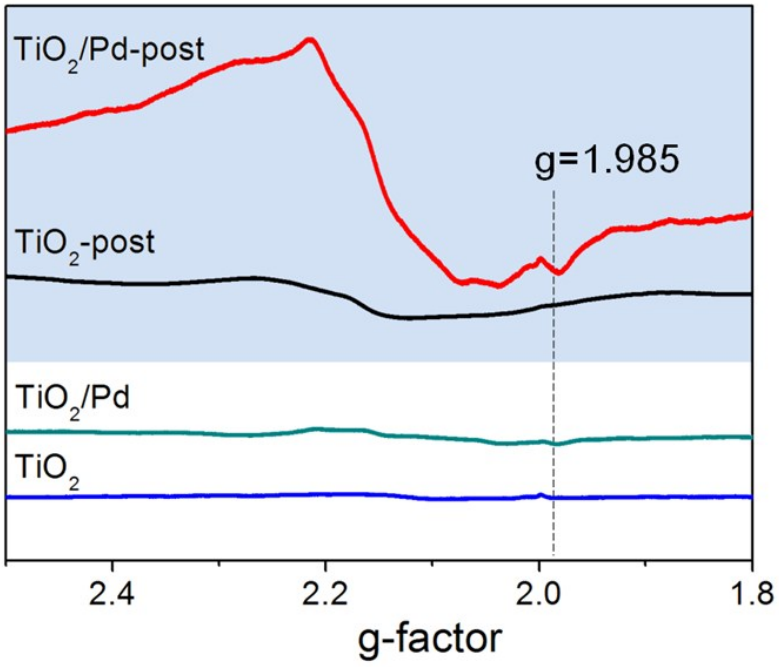

Figure S3. EPR spectra of different samples measured at 100 K. The asymmetric EPR signals at g = 1.98 of TiO_2/Pd-post sample should be ascribed to the Ti^{3+} species,[6] which were absent in either TiO_2/Pd, or pure TiO_2 before and after the hydrogen evolution experiment (TiO_2-post), implying that TiO_2/Pd was irreversibly reduced during the photocatalytic water splitting process.

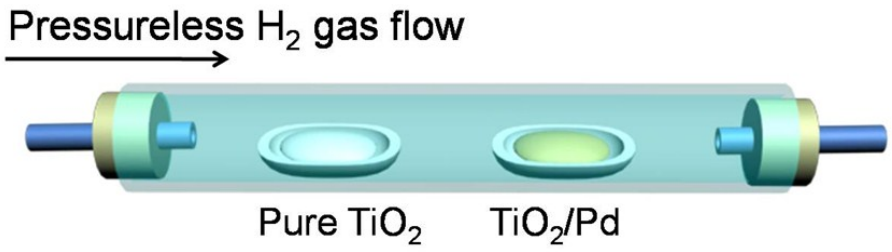

Figure S4. Schematics for the facile hydrogenation of TiO_2 in the presence of Pd, in which ambient H_2/Ar (10%) gas flow is introduced to hydrogenate TiO_2 under room temperature under the presence of Pd.

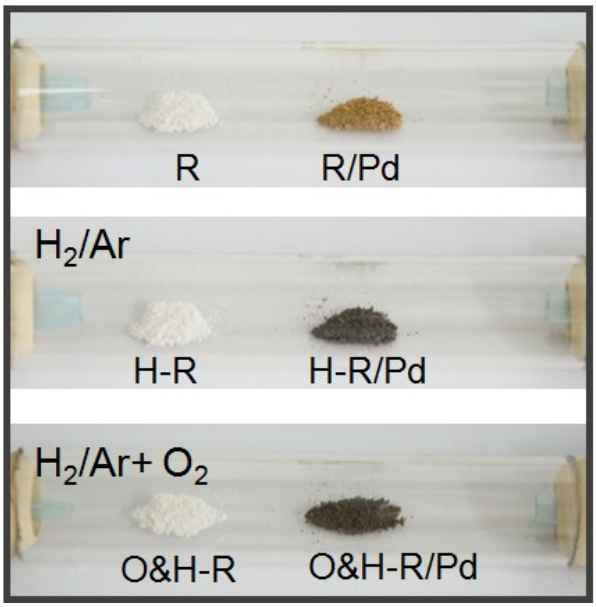

Figure S5. Digital photographs of R (left) and R/Pd (right) samples before (upper) and after Pd-catalyzed hydrogenation in H_2/Ar (middle) or in O_2 containing H_2/Ar (bottom) gas flows in 1 min. The colour of R/Pd changed into black immediately after the H_2 gas flow passed the sample.

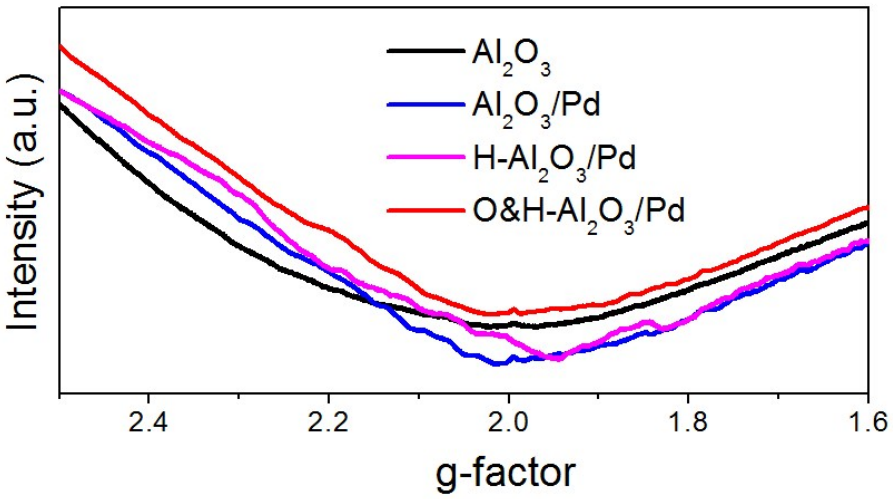

Figure S6. EPR spectra of α-Al_2O_3 and α-Al_2O_3/Pd samples after the same hydrogen treatments (H-Al_2O_3/Pd and O&H-Al_2O_3/Pd) measured at 100 K. No EPR signal can be detected after the hydrogen treatment of α-Al_2O_3/Pd, which suggests that all these created EPR signals observed in H-R/Pd and O&H-R/Pd samples are essentially from the TiO_2 matrix itself, excluding the contribution from the possible changes in chemical properties of Pd nanoparticles after H_2 treatment.

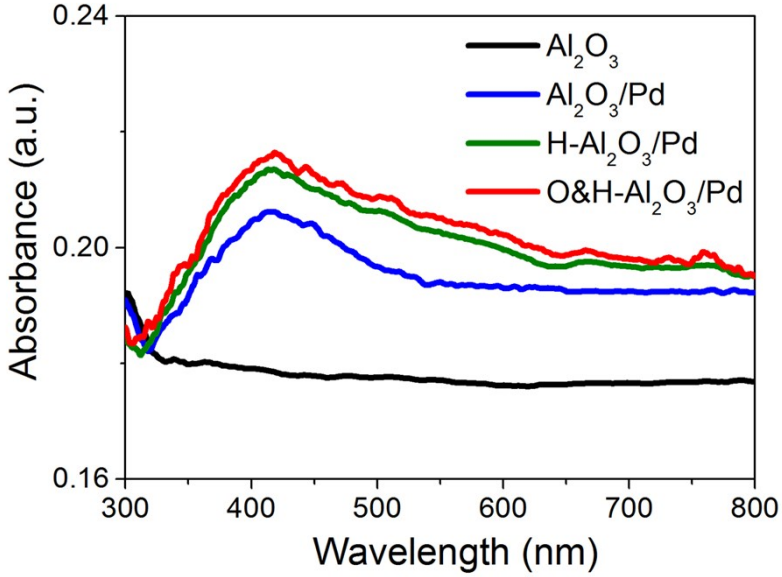

Figure S7. Diffuse reflectance UV-Vis spectra of different α-Al_2O_3 samples. The enhanced visible-light absorption of α-Al_2O_3/Pd should be attributed to the localized surface plasmon resonance of Pd nanoparticles.[7] However, similar UV-Vis spectra of α-Al_2O_3/Pd before and after the hydrogen treatments were obtained (H-Al_2O_3/Pd and O&H-Al_2O_3/Pd), indicating that the potentially changed chemical properties of Pd nanoparticles would not affect the light absorption property of the treated samples. Therefore, the remarkably enhanced visible light absorption of the obtained hydrogenated TiO_2 samples (Figure 1c) should be ascribed to the generated defects (Figure 1b), which could induce mid-gap states in TiO_2 to narrow its band gap (Figure 1d).

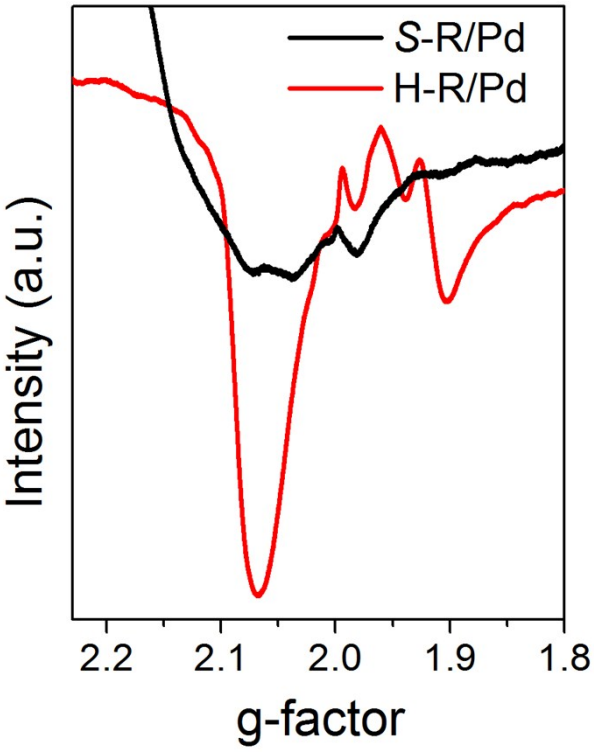

Figure S8. EPR spectra of self-reduced R/Pd sample (*S*-R/Pd) and H_2 treated R/Pd sample (H-R/Pd) measured at 100 K. The signal at g=1.96 is attributed to Ti^{3+} species, and the resonances at g values in the range of 2.02 to 2.12 are attributed to oxygen vacancies. Since the intensity of the signal is in positive correlations with the density of the corresponding species, the higher densities of oxygen vacancies and Ti^{3+} species are believed to have been generated in the hydrogenated R/Pd (H-R/Pd) sample than the self-reduced R/Pd sample (*S*-R/Pd).

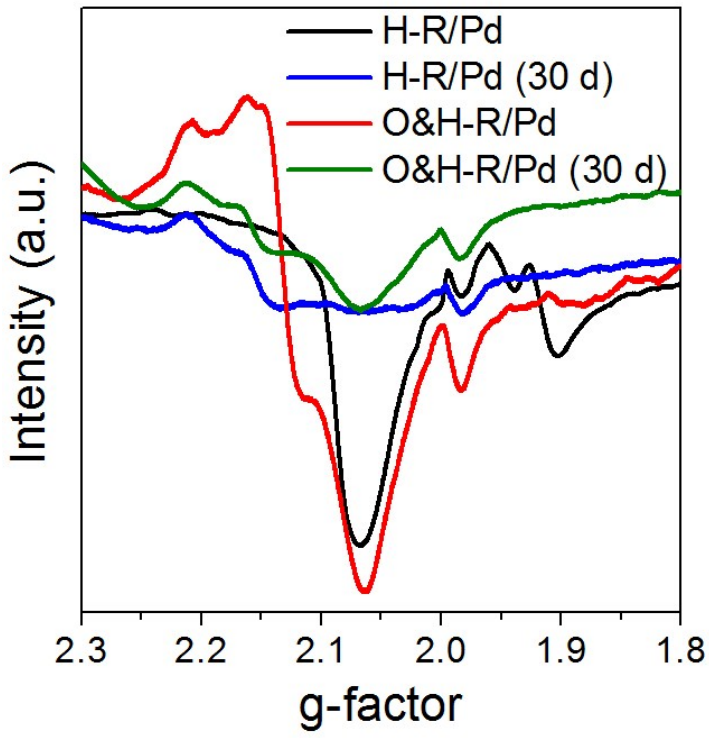

Figure S9. EPR spectra of freshly treated H-R/Pd and O&H-R/Pd samples and their corresponding 30-days-stored counterpart measured at 100 K. Even in 1 month, the Ti^{3+} species at g = 1.96 can still be detected in both H-R/Pd and O&H-R/Pd, indicating the long-term stability of the obtained hydrogenated TiO_2 through the present hydrogenation method.

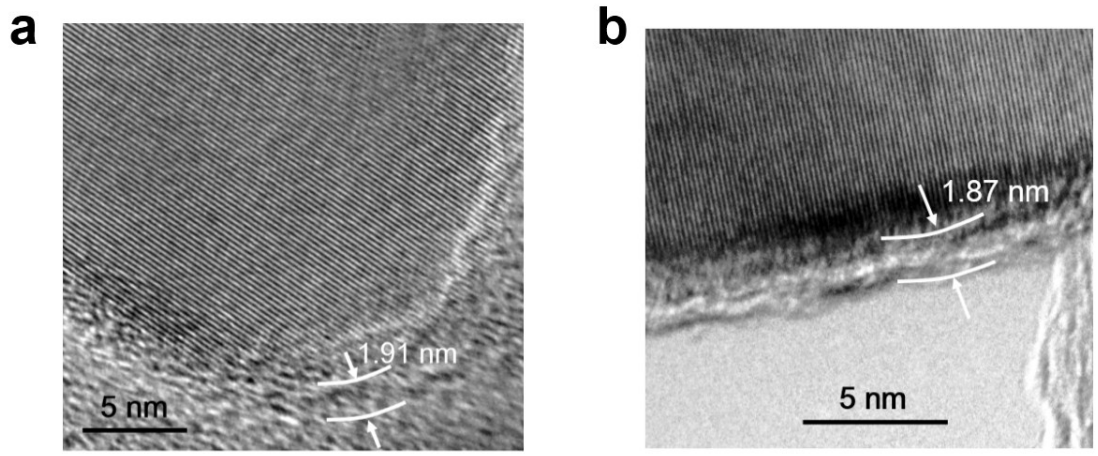

Figure S10. HRTEM image of O&H-R/Pd (a) and after 1 year storage in air atmosphere (b). The disordered surface was still retained with similar thickness, which indicates the stability of the unique crystalline core/disordered shell structure created through the oxygen-assisted Pd-catalyzed hydrogenation strategy.

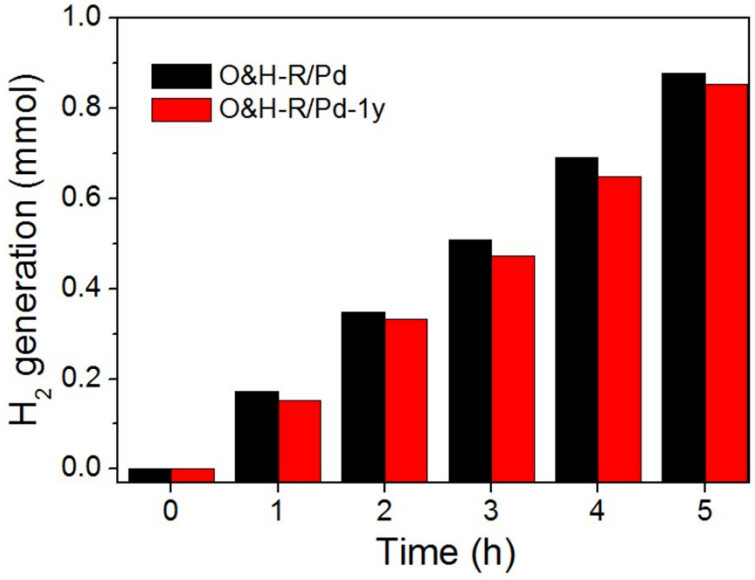

Figure S11. Photocatalytic hydrogen productions of O&H-R/Pd under AM 1.5 irradiation after 1 year storage in air atmosphere. Due to the stability of the disordered shell structure, the enhanced photocatalytic hydrogen production of O&H-R/Pd have been well retained in 1 year storage.

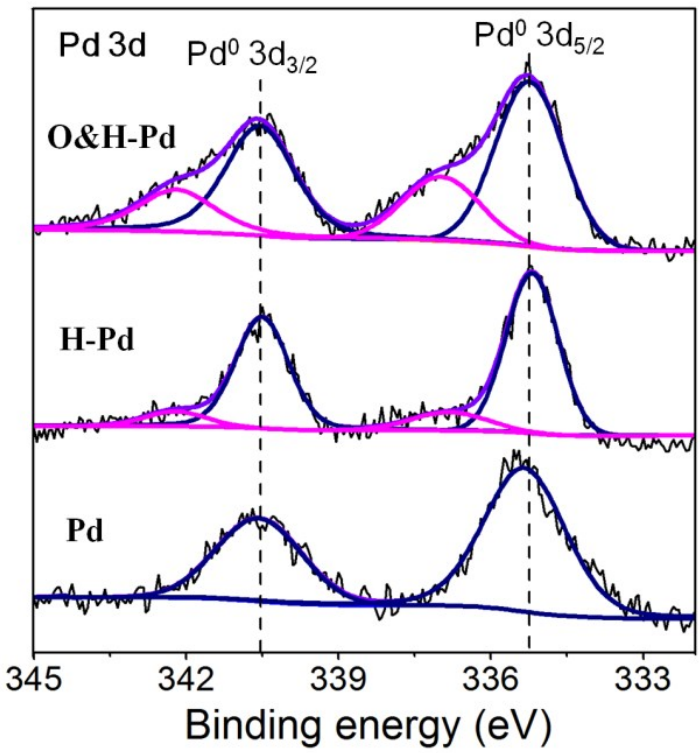

Figure S12. XPS spectra of Pd after the hydrogen (H-Pd) and oxygen-assisted hydrogen (O&H-Pd) treatments at room temperature. The appearance of new Pd peaks with higher chemical shifts in both H-Pd and O&H-Pd indicates the generation of high-valence state Pd species, which should arise from the formed PdH_x species with spontaneously dissociative hydrogen. Correspondingly, with the oxygen-assisted hydrogen treatment, O_2 will inevitably react with a small portion of the dissociated H atoms due to its extremely high activity and liberate a large amount of heat, which will efficiently accelerate this dissociation of H_2 into [H] and activate their diffusion to interact with the TiO_2 matrix.

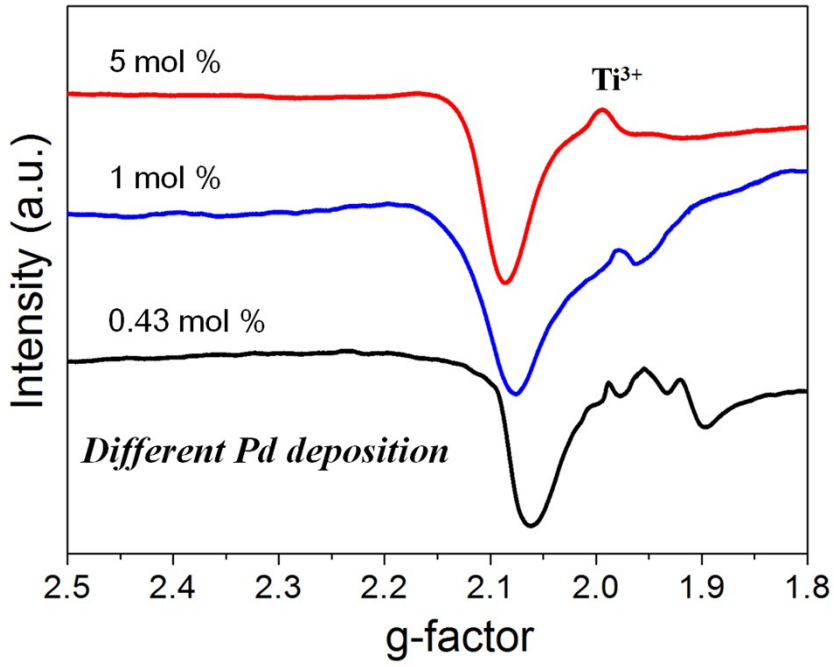

Figure S13. EPR spectra of different-amount Pd loaded rutile TiO_2 samples, varying from 0.43 mol % to 5 mol % Pd determined by ICP-OES, after treated with the same hydrogen gas flow (10 vol % H_2/Ar, 200 sccm, 10 min). The similar signal intensities of oxygen vacancies and Ti^{3+} species in different Pd loaded rutile TiO_2 samples were observed, indicating that the increased deposition amount of Pd could hardly induce more defects in TiO_2 via this hydrogenation process. As we know, the role of Pd is to catalyze the dissociation of molecular H_2 into highly active atomic hydrogen [H] species, which could further diffuse onto TiO_2 nanoparticles and react with them. Due to the highly efficient catalyzing effects of Pd nanoparticles, sufficient [H] species could be generated by the 0.43 mol % Pd loading amount, and increasing the deposition amount of Pd nanoparticles is therefore less significant in promoting the hydrogenation process of TiO_2 under these conditions.

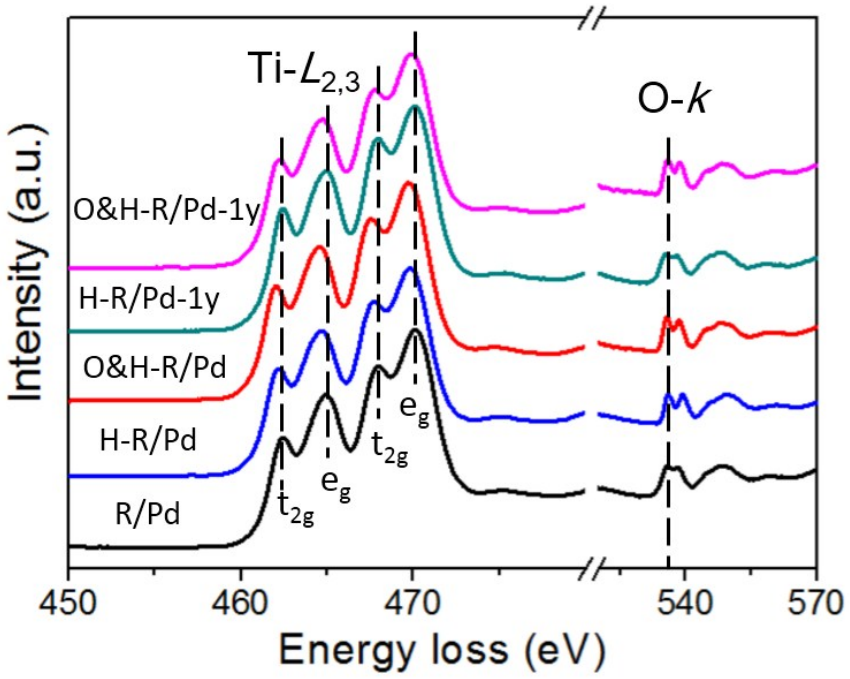

Figure S14. EELS spectra of different samples. After the Pd-catalyzed hydrogen treatments, the Ti-$L_{2,3}$ edge of TiO_2 shift towards low energy, indicating the generation of Ti^{3+} species.[8] And the lower energy shifts of Ti-$L_{2,3}$ edge in O&H-R/Pd than that in H-R/Pd suggests the higher concentration of Ti^{3+} species, further confirming the stronger reduction of titania by the accelerated dissociation of H_2 and the following hydrogenation due to the heating effect in the presence of oxygen introduced during preparing O&H-R/Pd. Meanwhile, compared with H-R/Pd after 1 year storage in air atmosphere, the Ti-$L_{2,3}$ edge of O&H-R/Pd still shifts towards low energy, suggesting the disordered surface of O&H-R/Pd could stabilize the reduced Ti^{3+} species under ambient conditions.

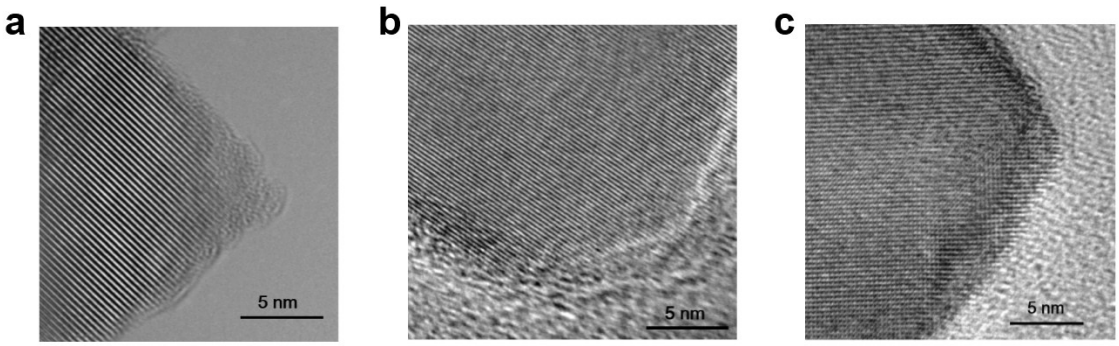

Figure S15. HRTEM images of rutile TiO_2 through the oxygen-assisted Pd-catalyzed hydrogenation treatments with varied oxygen concentrations of 1%, 2% and 4 % shown in a, b, c, respectively. When increasing the oxygen content from 1% to 2%, a slightly increased shell thickness (about 0.5 nm) was observed, which should be ascribed to the larger heat energy released during the reaction between [H] and O_2 to further accelerate the dissociation of H_2 into [H] species and reduce the TiO_2 matrix. However, when the oxygen content was further increased to 4%, disordered shell of the treated TiO_2 sample could be hardly detected because of the over-consumption of discrete [H] species by O_2, leading to insufficient [H] species to react with TiO_2 and to generate disordered surface shell.

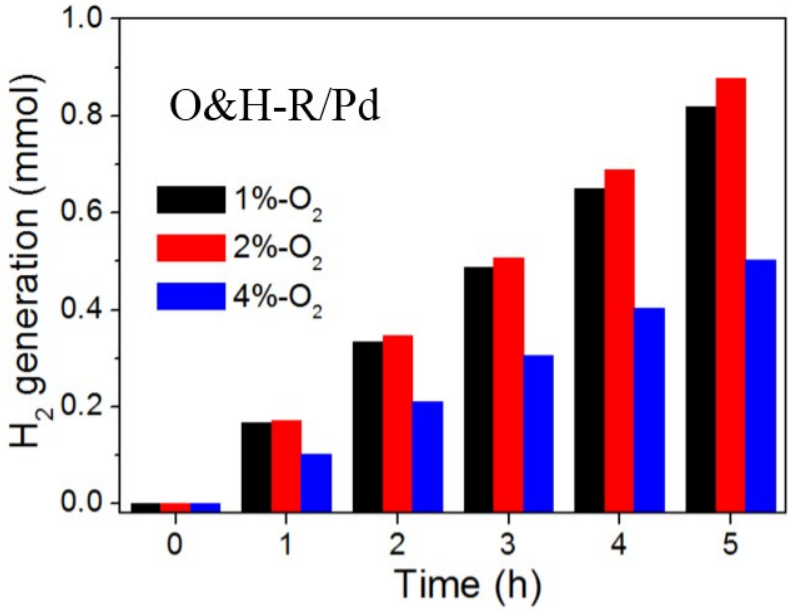

Figure S16. Photocatalytic hydrogen productions under AM 1.5 irradiation from O&H-R/Pd samples produced by introducing different O_2 amounts during the Pd-catalyzed hydrogen treatments. Although the increased disordered shell thickness was observed when increasing the oxygen content from 1% to 2% with the same H_2 treatment conditions (Figure S15), their photocatalytic hydrogen evolution rates were almost equivalent. This is because that, theoretically, heterogeneous photoreaction only takes place on the surface of photocatalysts, thus increasing the thickness of disordered shell could hardly result in further enhanced photocatalytic activity of the catalyst. When the oxygen content was further increased to 4%, the photocatalytic hydrogen evolution rate was largely decreased due to the absence of disordered surface shell. Therefore, in the oxygen-assisted Pd-catalyzed hydrogenation process, the amount of O_2 should be carefully controlled low enough to avoid the over-consumption of discrete [H] species by introduced O_2.

Table S2. Statics of disordered shell thicknesses and photocatalytic H_2 production rates of O&H-R/Pd produced by introducing different O_2 concentrations during the Pd-catalyzed hydrogen treatments.

Different O_2 content for O&H-R/Pd	1%	2%	4%
Disordered shell thickness (nm)	1.1±0.23	1.8±0.37	---
Photocatalytic H_2 production (mmol g^{-1} h^{-1})	3.15	3.51	2.01

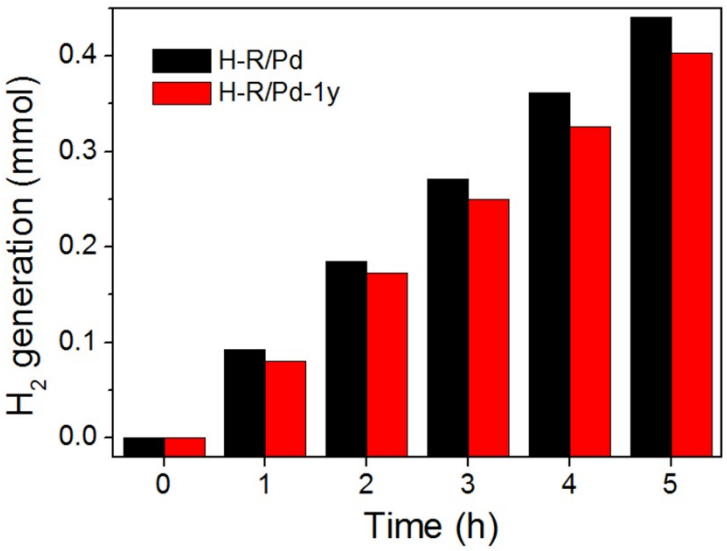

Figure S17. Photocatalytic hydrogen productions of H-R/Pd under AM 1.5 irradiation after 1 year storage in air atmosphere. Although the point defects of H-R/Pd such as oxygen vacancies and Ti^{3+} species decayed during long time exposure in air (Figure S9, S14), the photocatalytic hydrogen evolution activity was still maintained, which should be ascribed to the self-reduction effect in the presence of Pd to induce the defects during the H_2 evolution experiment.

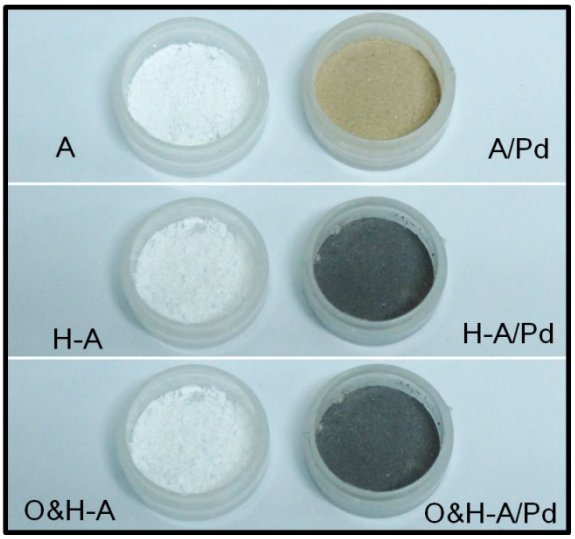

Figure S18. Digital photographs of A (left) and A/Pd (right) samples before (upper) and after Pd-catalyzed hydrogenation in H_2/Ar (middle) or in O_2 containing H_2/Ar (bottom) gas flows in 1 min.

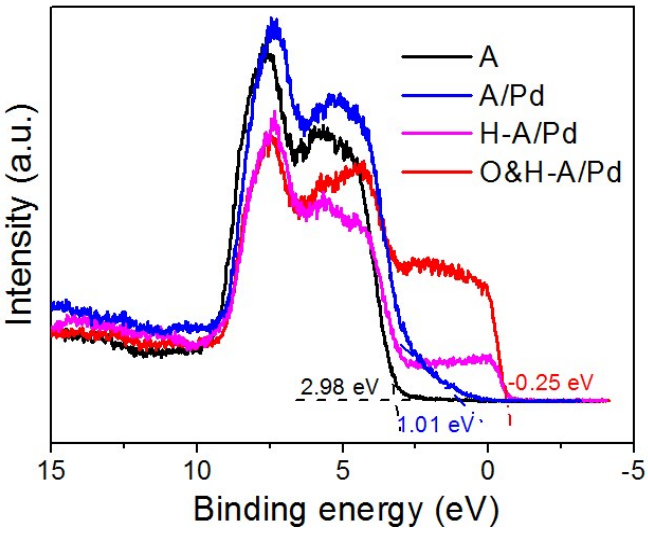

Figure S19. Valence-band XPS spectra of different anatase TiO_2 samples. The significant blue-shifts VBM of H-A/Pd and O&H-A/Pd samples toward the vacuum level suggest the generated defects via the Pd-catalyzed hydrogenation treatment inducing mid gap states in anatase TiO_2 samples, leading to the significantly enhanced visible light absorption.

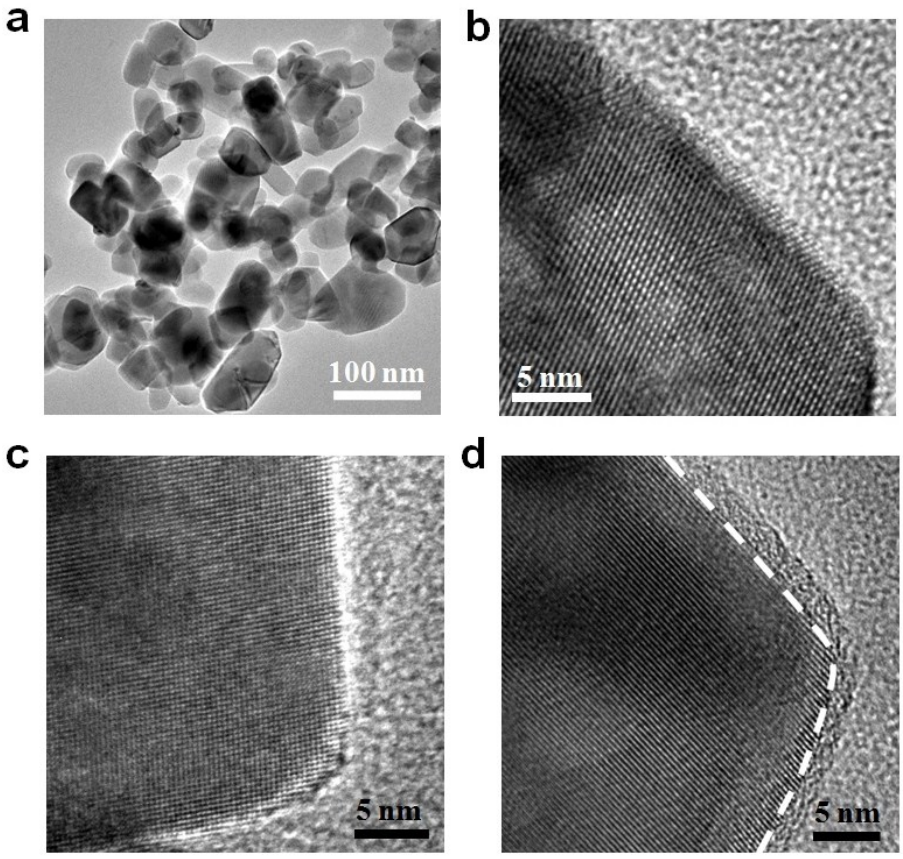

Figure S20. Morphological and microstructural characterizations of different anatase samples. Overview TEM image (a) and HRTEM image (b) of A/Pd sample. HRTEM images of H-A/Pd sample (c) and O&H-A/Pd sample (d). Note that in contrast to the well-crystallized feature of other samples, O&H-A/Pd shows a noticeable disordered shell of 3 nm in thickness on the surface of the well-crystallized TiO_2 core, indicating the lattice reconstruction of anatase TiO_2 after the oxygen-assisted Pd-catalyzed hydrogenation process.

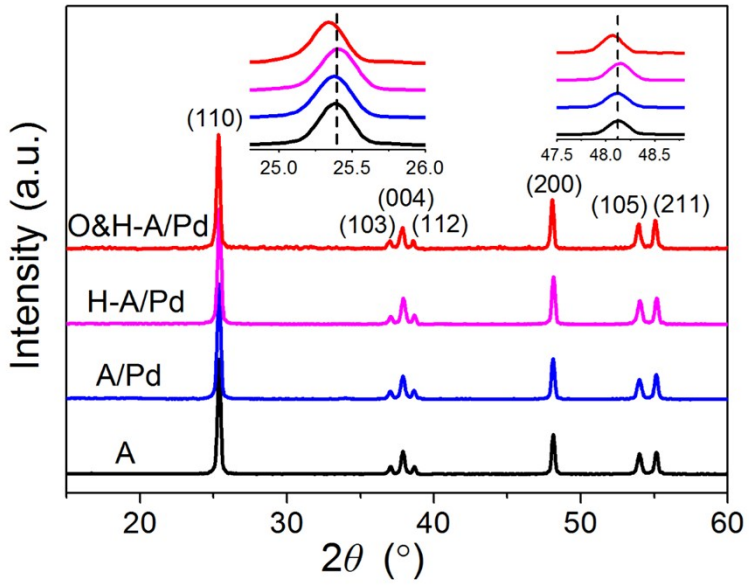

Figure S21. XRD patterns of different anatase TiO_2 samples, indicating their highly crystallized features. The peak shifts of O&H-A/Pd towards lower angle should be ascribed to the lattice expansion in the amorphous surface layer.

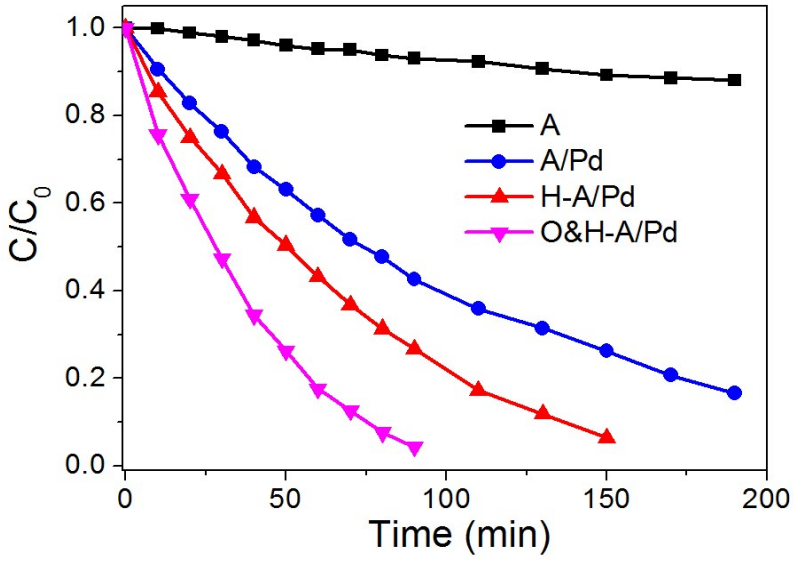

Figure S22. Photocatalytic degradation of a methylene blue solution by different anatase TiO_2 samples in the aerobic condition under AM 1.5 G illumination. The obtained hydrogenated TiO_2 exhibited substantially improved photocatalytic activities and the unique crystalline core/disordered shell structure of O&H-A/Pd sample can further improve its solar energy utilization under aerobic conditions.

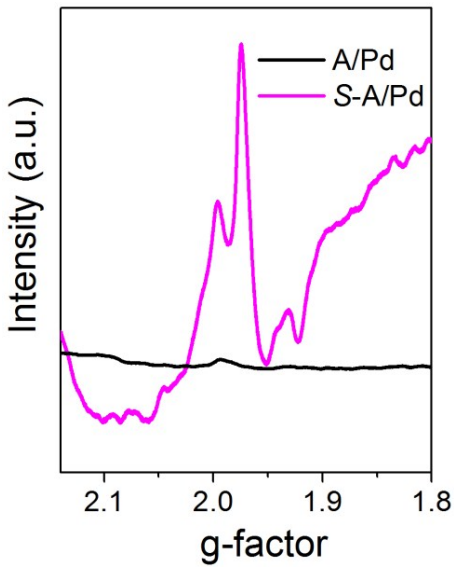

Figure S23. EPR spectra of A/Pd sample before (black line) and after (red line) the photocatalytic hydrogen evolution experiments under AM 1.5 G irradiation. The signal at g = 1.96 is attributed to Ti^{3+} species, and the resonances at g values in between 2.02 to 2.12 are attributed to oxygen vacancies, indicating that A/Pd sample has been reduced during the hydrogen evolution experiment.

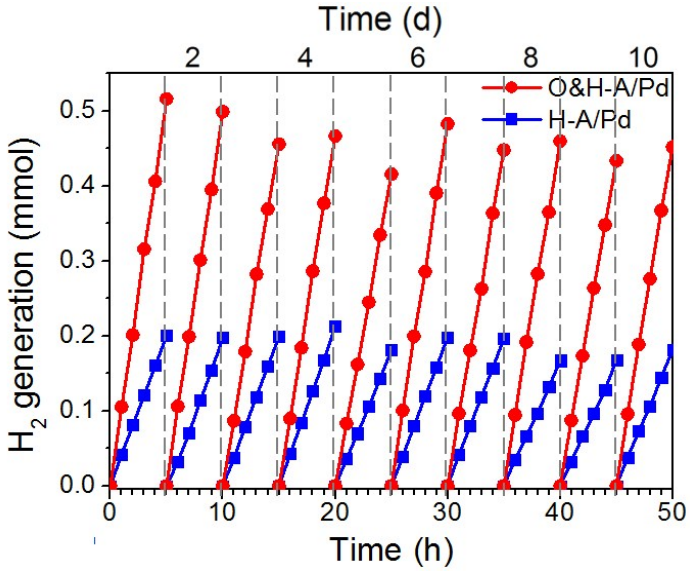

Figure S24. Cycling measurements of photocatalytic hydrogen evolution from H-A/Pd and O&H-A/Pd under AM 1.5 G illumination, similar H_2 generation rate was observed during the long-term photocatalytic tests confirming the photocatalytic stability of the obtained hydrogenated anatase TiO_2.

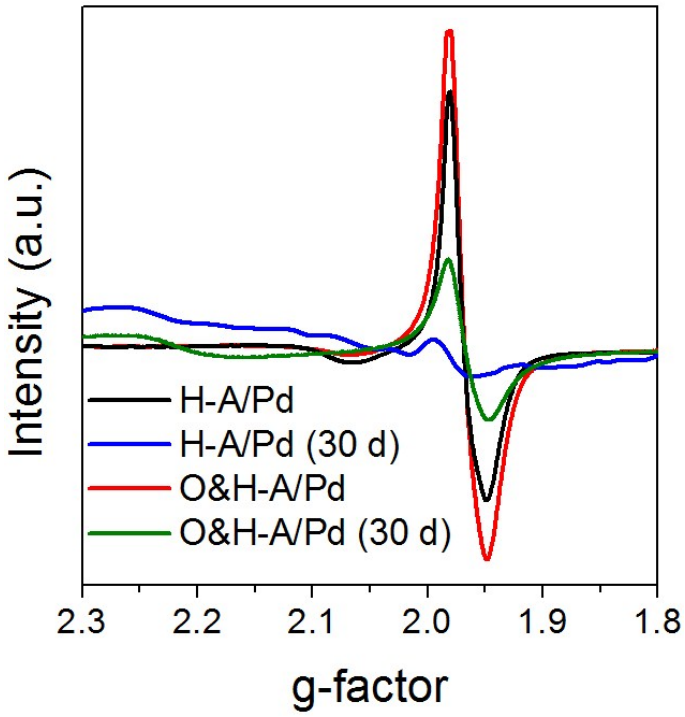

Figure S25. EPR spectra of fresh H-A/Pd and O&H-A/Pd samples and their corresponding 30-days-stored counterparts measured at 100 K. Even in 1 month, the Ti^{3+} species can still be detected in both H-A/Pd and O&H-A/Pd, indicating the long-time stability of the obtained hydrogenated TiO_2 through the present Pd-catalyzed hydrogenation method. In addition, the signal intensity of Ti^{3+} species in O&H-A/Pd sample is considerably higher than that in H-A/Pd sample, implying that the disordered surface is helpful for the long-term stability of the obtained hydrogenated anatase TiO_2.

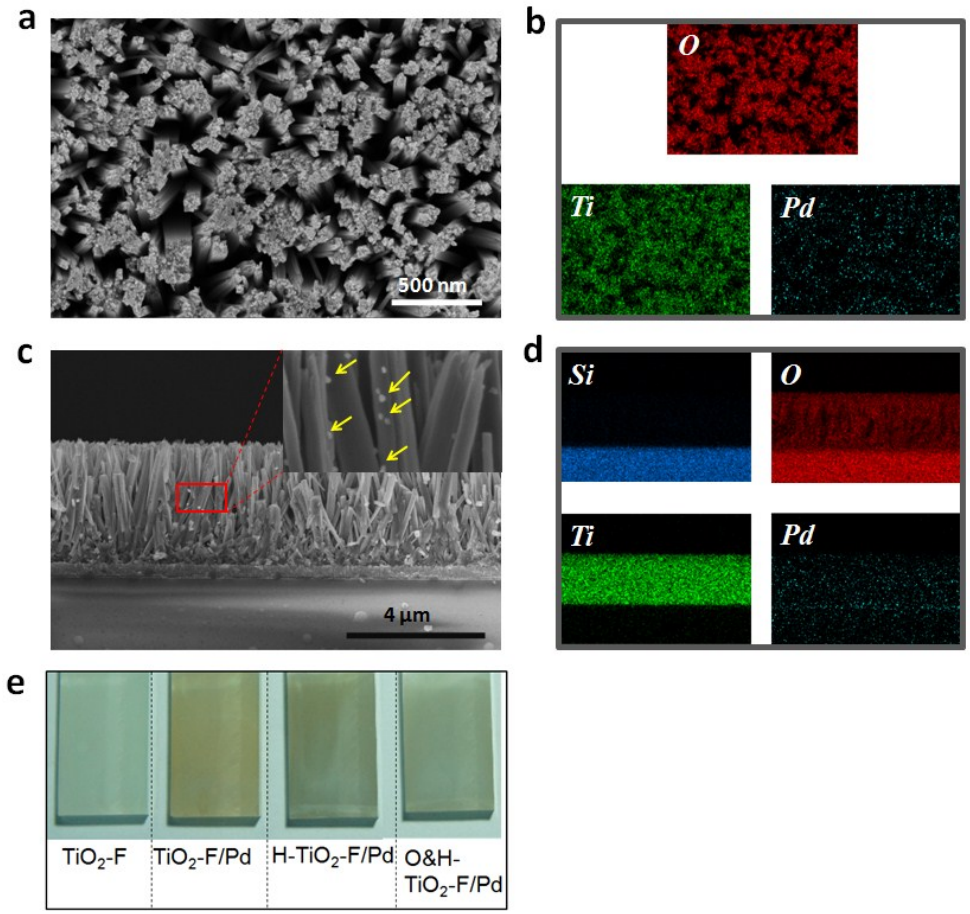

Figure S26. Top-view (a) and side-view (c) SEM images of O&H-TiO_2-F/Pd sample and the corresponding elemental mappings (b for a, d for c). The insert in c is the backscattered electron (BSE) zoom-in image of the marked region. The yellow arrows highlight the Pd nanoparticles on the TiO_2 nanoarrows, implying that Pd NPs are well-dispersed on TiO_2 nanowires. And from the side-view SEM image, O&H-TiO_2-F/Pd sample remains intact without detectable damage post the oxygen-assiated self-heating process. (e) Photographs of differently treated TiO_2 films, the colour of TiO_2-F/Pd changes from light yellow to black after the mild hydrogen treatment, indicating the improved visible light absorption of TiO_2 nanowires through the facial Pd-catalyzed hydrogenation treatment.

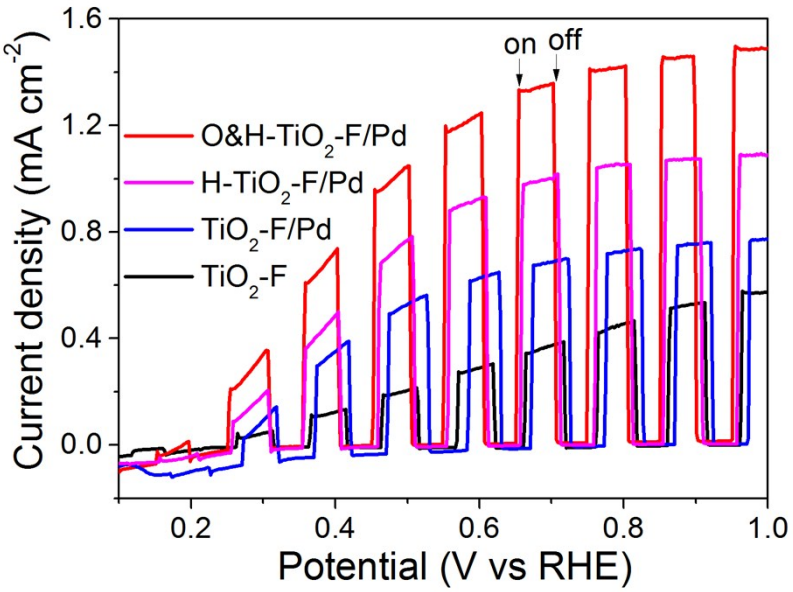

Figure S27. *J-V* curves obtained on different TiO_2 films under the chopped AM 1.5 G illumination at a scan rate of 5 mV s^{-1}. The dark current densities in all cases are negligible and the photocurrent densities of O&H-TiO_2-F/Pd sample are almost doubled compared with those of TiO_2-F/Pd sample.

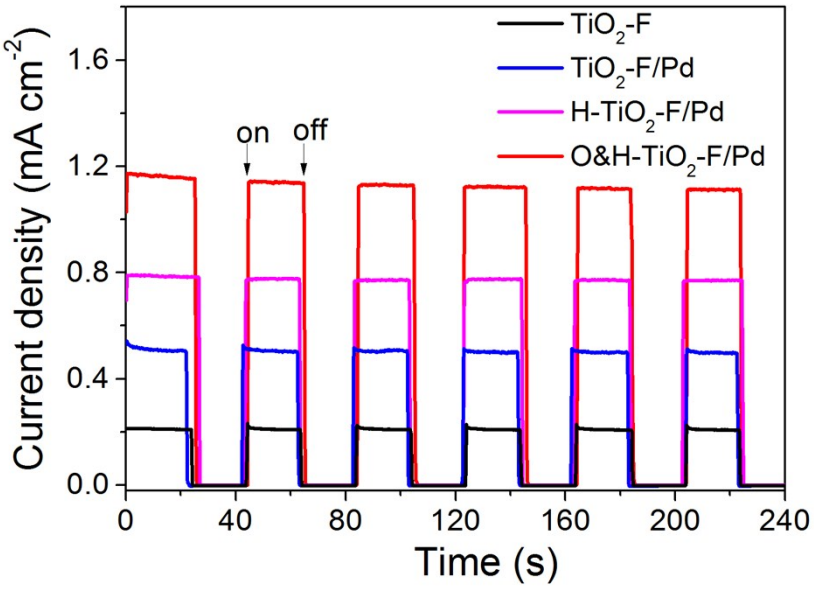

Figure S28. Transient photocurrent curves of different TiO_2 films under chopped AM 1.5 G illumination at 0.5 V vs RHE, showing the prompt and reproducible photo responses of O&H-TiO_2-F/Pd and H-TiO_2-F/Pd samples upon illumination. The steady-state photocurrent densities of H-TiO_2-F/Pd and O&H-TiO_2-F/Pd samples are about 1.34 and 2 times that of TiO_2-F/Pd sample, respectively.

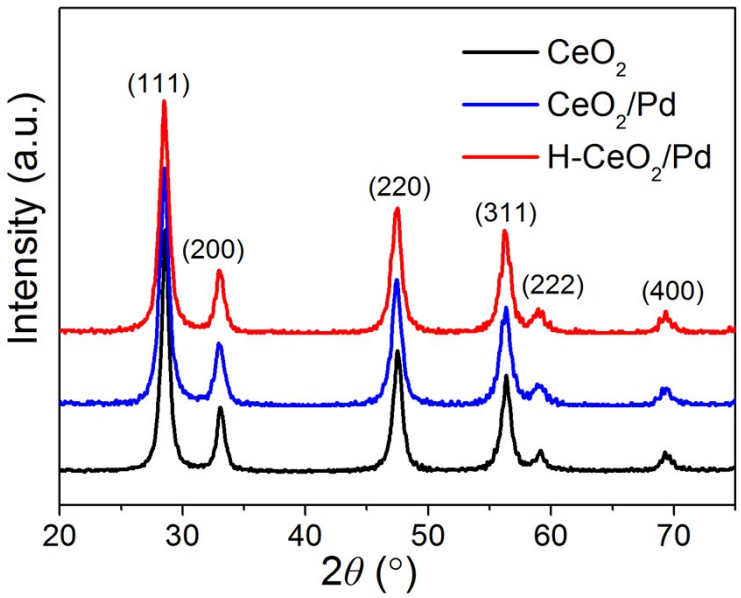

Figure S29. XRD patterns of different as-synthesized CeO_2 samples. All of the samples exhibit typical CeO_2 XRD patterns (PDF 04-0593) without any other phases.

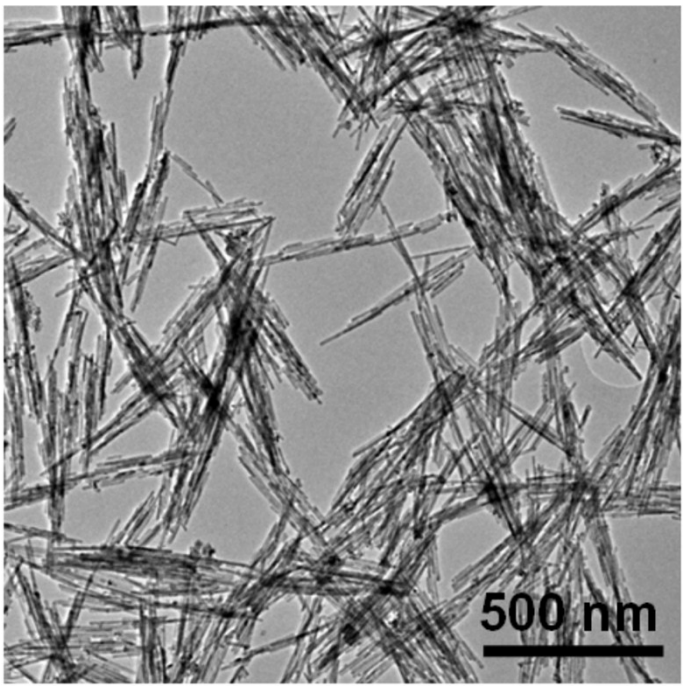

Figure S30. Overview TEM image of the Pd-incorporated CeO_2 sample. The CeO_2 sample was synthesized as 1D nanowire with the length around 400 nm. It is hard to find Pd nanoparticles from the TEM overview due to the low Pd doping amount.

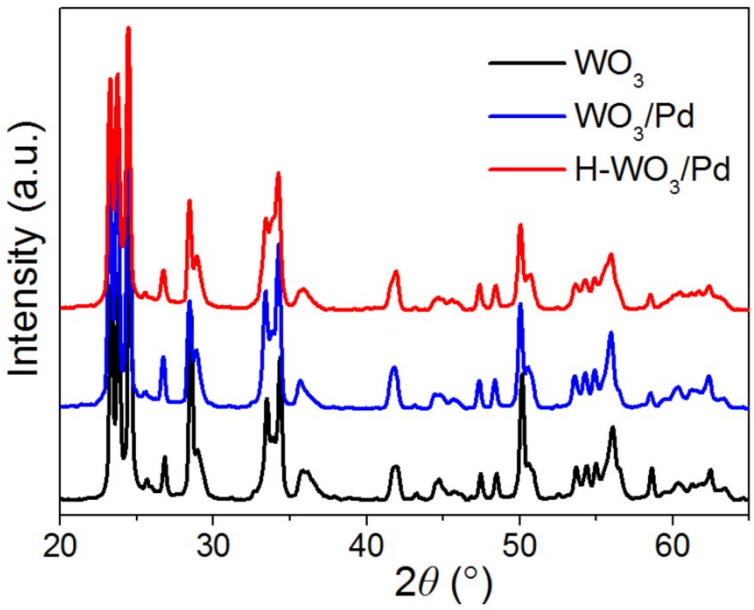

Figure S31. XRD patterns of different as-synthesized WO_3 samples. All of the XRD patterns belong to WO_3 samples (PDF 20-1324) without any other phases.

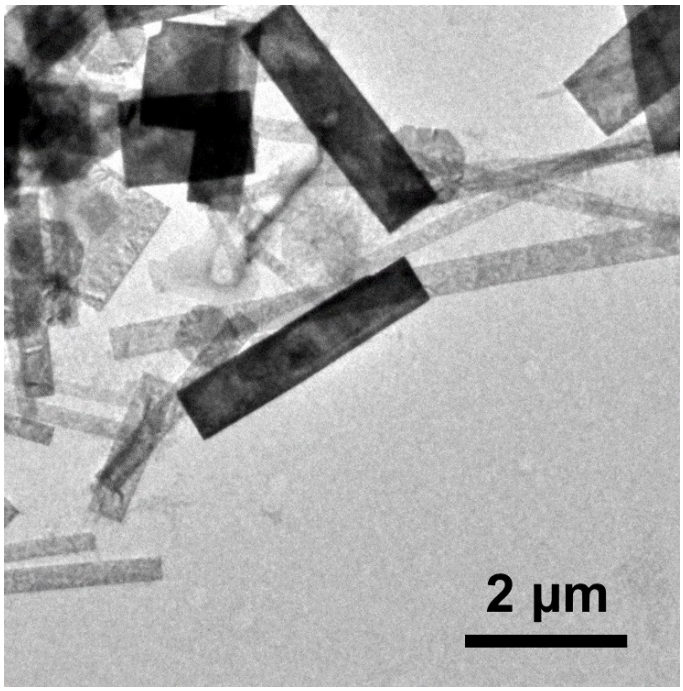

Figure S32. Overview TEM image of the Pd doped WO_3 microrods. Due to the low Pd doping amount, it is hard to find Pd nanoparticles from the TEM overview.

3. Supplementary References

1. M. Wu, G. Lin, D. Chen, G. Wang, D. He, S. Feng and R. Xu, *Chem. Mater.*, 2002, **14**, 1974-1980.
2. X. Han, Q. Kuang, M. Jin, Z. Xie and L. Zheng, *J. Am. Chem. Soc.*, 2009, **131**, 3152-3153.
3. B. Liu and E. S. Aydil, *J. Am. Chem. Soc*., 2009, **131**, 3985-3990.
4. W. Gao, J. Li, X. Zhou, Z. Zhang, Y. Ma and Y. Qu, *J. Mater. Chem. C*, 2014, **2**, 8729-8735.
5. G. F. Cai, J. P. Tu, D. Zhou, L. Li, J. H. Zhang, X. L. Wang and C. D. Gu, *CrystEngComm*, 2014, **16**, 6866.
6. D. C. Hurum, A. G. Agrios, S. E. Crist, K. A. Gray, T. Rajh and M. C. Thurnauer, *J. Electron Spectrosc*., 2006, **150**, 155-163.
7. L. Christoph, Y. Zhe, Z. Igor and K. Bengt, *Nano Lett.*, 2006, **6**, 833-838.
8. C. M. Wang, Z. Yang, S. Thevuthasan, J. Liu, D. R. Baer, D. Choi, D. Wang, J. Zhang, L. V. Saraf and Z. Nie, *Appl. Phys. Lett.*, 2009, **94**, 233116.